



Pt nanoparticles in polyelectrolyte multilayers: Polymer effects on the electrocatalytic activity for methanol oxidation



Santiago E. Herrera, Mario Tagliazucchi, Federico J. Williams, Ernesto J. Calvo

Departamento de Química Inorgánica, Analítica y Química Física, INQUIMAE-CONICET, Facultad de Ciencias Exactas y Naturales, Universidad de Buenos Aires, Pabellón 2, Ciudad Universitaria, Pabellón 2, Buenos Aires C1428EHA, Argentina

ARTICLE INFO

Keywords:

Self-assembly
Polyelectrolyte multilayer
Platinum nanoparticles
Methanol oxidation
Electrocatalysis

ABSTRACT

The layer-by-layer (LbL) self-assembly technique is a simple and versatile tool for the controlled chemical conversion of metal ions into nanoparticles. In this work, we prepared LbL thin films containing Pt nanoparticles electroactive towards electro-oxidation of methanol by a two-step process, involving the exchange of different Pt precursor ions into the film, followed by their chemical reduction. We addressed the influence of the Pt precursor ($\text{Pt}(\text{NH}_3)_4^{2+}$ and PtCl_6^{2-}) and polyelectrolyte-pairs (poly(diallyldimethylammonium chloride) (PDDA)/Nafion and poly(allylamine hydrochloride) (PAH)/poly(acrylic acid) (PAA)) on the properties and electrocatalytic activity of the nanoparticles. NPs synthesized from $\text{Pt}(\text{NH}_3)_4^{2+}$ outperformed those growth from PtCl_6^{2-} , the precursor used in previous works to prepared Pt NPs within LbL films. The combination of $\text{Pt}(\text{NH}_3)_4^{2+}$ and PDDA/Nafion films produced the best electrocatalytic performance with a specific activity of 0.8 mA.cm^{-2} . By varying the number of exchange/reduction cycles (n) between 1 and 5, a marked increase in the catalytic activity was observed for the first 2 cycles, followed by a saturation regime. The peak potential of the Pt/Pt oxide peak also increases in the first cycles and approaches a constant value close to that of a bulk Pt electrode coated with PDDA/Nafion. These behaviors are explained in terms of a strong polymer-Pt surface interaction that decreases with increasing n and stabilizes for $n > 2$.

1. Introduction

The chemical conversion of precursor ions confined in polyelectrolyte multilayer films is a promising and flexible route to modify almost any surface with functional nanoparticles (NPs) [1–10]. This nanoreactor strategy was pioneered by Rubner's and Cohen's groups, who confined metal ions in preformed nanoreactor polyelectrolyte films and transformed them into NPs by chemical reduction or precipitation [1]. In this method, the exchange/reduction cycle can be repeated to increase NP loading [1,2]. Bruening and coworkers disclosed an alternative procedure involving co-assembly of metal ions and polyelectrolytes and subsequent formation of NPs [3]. In both procedures, the layer-by-layer (LbL) processing offers a great design flexibility given by the choice of the type and number of layers, the assembly pH and ionic strength, the charge of the topmost layer, etc. This wide spectrum of variables allows control over the properties of the film and the NPs. For instance, the NP size can be tuned by adjusting the number of exchange/reduction cycles [2], the assembly pH [2,4], the exchange and reduction conditions, and the metal ion concentration [8].

In order to obtain metal NPs using an LbL film as nanoreactor, transition metal ions must be first integrated in the supramolecular structure of the multilayer. Among the different strategies available, the use of metallo-polyelectrolytes [11–13] and post-complexation of transition metals by ion exchange [1–4] are the most reliable techniques. The latter case is a simple and versatile method that relies on two main interactions: i) exchange of the original ligands that complex the metal ion in solution with available ligands (Lewis bases) covalently bound to the polymers, and/or ii) electrostatic binding between charged polyelectrolytes and oppositely charged metal ions [14]. For this reason, the loading of metal ions into the LbL film depends both on the nature of the polyelectrolyte and the transition metal complexes used in the loading stage. For example, Mentbayeva and coworkers studied the incorporation of Co^{2+} and Cu^{2+} into films made of different polyelectrolyte-pairs using branched polyethyleneimine (PEI) or quaternized poly-4-vinylpyridines (QPVPs) as polycations and poly(acrylic acid) (PAA) or poly(styrene sulfonate) (PSS) as polyanions, and showed that the amount of metal ions loaded into the film strongly depended on the type of polyelectrolyte, the assembly pH, and the fraction of charge of the polymer [15].

E-mail address: sherrera@qi.fcen.uba.ar (S.E. Herrera)

<https://doi.org/10.1016/j.jelechem.2023.117430>

Received 24 February 2023; Received in revised form 1 April 2023; Accepted 5 April 2023

Available online 13 April 2023

1572-6657/© 2023 Elsevier B.V. All rights reserved.

The applications of metallic NPs grown within LbL nanoreactors are numerous: Ag NPs were studied for biocide surfaces [3,5,16], Au, Pd and Pt for O₂ reduction reaction and methanol oxidation reaction (MOR) [3,17–19], Pd NPs for catalytic and electrocatalytic hydrogenations [7–9,20], and bimetallic NPs for catalysis [21–23]. Zhang et al. reported the preparation of Pt NPs by ion exchange of PtCl₆²⁻ in PSS/poly(diallyldimethylammonium chloride) (PDDA) films supported on indium tin oxide, followed by *in situ* chemical reduction with NaBH₄ [24]. These Pt NPs showed a promising electrocatalytic activity towards MOR and an increase of the oxidation current with increasing number of exchange/reduction cycles. Wang et al., on the other hand, studied the impact of different synthesis parameter (salt concentration, reduction time and temperature) on the size of Pt clusters made from PSS/PDDA films and PtCl₆²⁻ [25]. More recently, by using polyelectrolyte-coated titanium carbide (Ti₃C₂T_x) MXene nanosheets, Huajie Huang et al. reported the formation of electroactive Pd nanoworms [26], Pt nanowires [27], and Pt-on-Pd nanodendrites [28]. Here, metal precursors were first loaded into the interface of MXene nanosheets by interaction with polyelectrolytes and then were reduced to form metal NPs. All MXene-based electrocatalysts displayed superior electrocatalytic activity towards MOR with enhanced long-term stability. Moreover, MXene nanosheets were shown to be highly versatile materials to act as nanoreactors for the synthesis of different MOR-active metal nanoparticles [27,29].

The interest in the nanoreactor scheme for the preparation of Pt NPs resides in its ability to control NP size, dispersion and activity, characteristics not always present in standard preparation routes such as electrodeposition, impregnation-reduction and NP synthesis in solution [30]. As discussed above, the role of the polyelectrolyte film in confining the metal-complex precursors—either by electrostatic interactions or ligand-exchange reactions—is well recognized. Much less is known about the effect of the polyelectrolyte matrix on the catalytic performance of embedded NPs. In this work, we studied the preparation of Pt NPs within two different types of LbL films and using two different Pt precursors. We show that, when Pt NPs are prepared using Pt(NH₃)₄²⁺, the specific electrocatalytic activity for MOR outperforms that of NPs prepared from PtCl₆²⁻ (which was the precursor used in the previous works of Zhang et al. and Wang et al.) [24,25]. This effect is ascribed to the detrimental effect of chloride ions on the performance of the reaction. We also show that NPs prepared within poly(allylamine hydrochloride) (PAH)/(PAA) films have a smaller specific electrocatalytic activity than NPs prepared within PDDA/Nafion multilayers, which in turn have smaller specific activity than a bare Pt electrode. We explain this result as a negative effect of the polymer-NP interactions on MOR. Noteworthy, this deleterious effect is mitigated when increasing the number of exchange/reduction cycles, which increases the specific electrocatalytic activity of the NPs.

2. Experimental

2.1. Materials

The following chemicals were used without further purification: Poly(acrylic acid) (PAA) (35 wt% in H₂O, Mw ~ 100000, Aldrich); poly(diallyldimethylammonium chloride) (PDDA) (20 wt% in H₂O, Mw ~ 150000, Aldrich), poly(allylamine hydrochloride) (PAH) (Mw 56000, Aldrich), Nafion (purum, ~5 wt% in lower aliphatic alcohols and water, Aldrich), chloroplatinic acid hexahydrate H₂PtCl₆·6H₂O (Aldrich), tetraammineplatinum(II) nitrate Pt(NH₃)₄(NO₃)₂ (Aldrich), sodium borohydride NaBH₄ (Aldrich), H₂SO₄ (Cicarelli), MeOH (HPLC, J. T. Baker). The polyelectrolytes solution concentration was 20 mM for PAH, PDDA and PAA, and 1 mg ml⁻¹ for Nafion, without added salt except for the HCl or NaOH required to bring the solutions to the final pH (7 for Nafion, 8 for PAH, 4 for PAA and 7 for PDDA). All solutions were prepared with 18 MΩ

Milli-Q® (Millipore) water. Nafion solution was prepared using a 1:1 vol mixture of H₂O/EtOH.

2.2. Multilayer assembly and nanoparticle synthesis

Compact Graphite Plates (AXF-5QCF, POCO Graphites) were used as supports for multilayer assembly. The substrate was cut into pieces of 20 mm × 10 mm, sequentially polished with 1, 0.3 and 0.05 μm alumina powder, sonicated in isopropyl alcohol for 10 min and rinsed with Milli-Q water. Multilayer assembly was performed by alternate immersion in continuously stirred polyelectrolyte solutions (10 mM, monomer concentration), starting from the positively charged polymer. Between adsorption steps, graphite substrates were washed twice in Milli-Q water with mechanical stirring for 15 min. The capping layer of the multilayers films was chosen to bear a charge of opposite sign to that of the Pt precursor (*i.e.* LbL films were terminated in the polycation for PtCl₆²⁻ and in the polyanion for Pt(NH₃)₄²⁺).

Pt NPs were synthesized by immersing the sample into a 10 mM solution of the Pt precursor for 24 h, thoroughly rinsed with water and reduced with NaBH₄ 100 mM at 80 °C for 5 min. This process was repeated the desired number of times.

2.3. Electrochemical experiments

Electrochemical measurements were carried out at room temperature with an Autolab PGSTAT 30 potentiostat (Autolab, Ecochemie) in a purpose built three electrode Teflon cell with an exposed area of 0.19 cm² delimited by an inert O-ring. The Ag/AgCl; 3 M KCl (0.210 V vs. NHE) reference electrode was placed in a glass tube containing the same solution as the cell and connected to it by a glass frit in order to avoid chloride contamination. All electrode potentials were quoted with respect to this reference electrode. A platinum gauze auxiliary electrode of large area was employed. All measuring solutions were purged with argon for a minimum of 20 min before each experiment and the measurements were carried out under that atmosphere. The electrochemically active Pt surface areas (ECSA) were estimated by hydrogen underpotential deposition using a relationship of 210 μC.cm⁻² [31,32].

2.4. X-Ray Photoelectron Spectroscopy

X-ray Photoelectron Spectroscopy measurements (XPS) were performed under UHV conditions (base pressure < 5 10⁻¹⁰ mbar) in a SPECS UHV spectrometer system equipped with a 150 mm mean radius hemispherical electron energy analyzer and a nine channeltron detector. XPS spectra were acquired at a constant pass energy of 20 eV using an un-monochromated MgKα (1253.6 eV) source operated at 12.5 kV and 20 mA and a detection angle of 30° with respect to the sample normal. Quoted binding energies are referred to the Au 4f_{7/2} emission at 84 eV. Atomic ratios were calculated from the integrated intensities of core levels after instrumental and photoionization cross-section corrections.

2.5. Scanning electron microscopy

Images were acquired with a FEG-SEM (Zeiss DSM 982 GEMINI, Carl Zeiss, Oberkochen, Germany) operating at 10 kV. An in-lens SE detector was used.

2.6. Ellipsometry

Film thickness for the Nafion/PDDA system was estimated from ellipsometric experiments performed on a HOPG substrate using a SenTech SE400 equipped with a 632.8 nm laser as polarized light source. After each adsorption step, the sample was rinsed with Milli-Q water and dried with N₂. Then, the ellipsometric parameters, ψ and Δ were

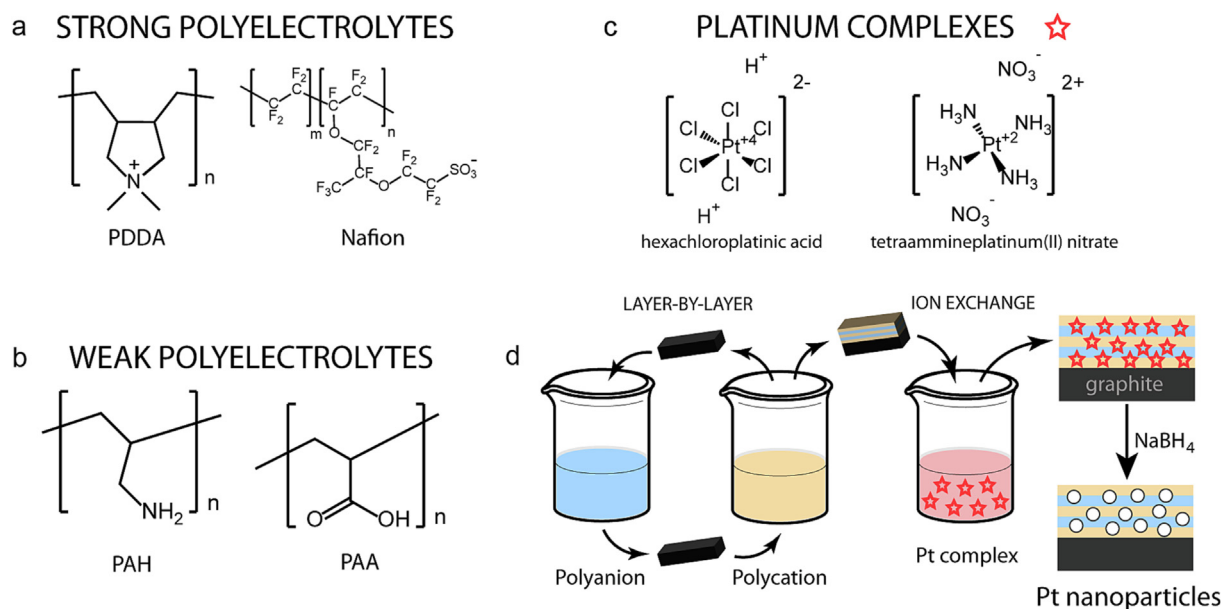


Fig. 1. Chemical structures of the strong polyelectrolytes PDDA and Nafion (a), the weak polyelectrolytes PAH and PAA (b), and the Pt complexes PtCl_6^{2-} and $\text{Pt}(\text{NH}_3)_4^{2+}$ (c) used for the construction of Pt NP-containing polyelectrolyte multilayer (d).

collected for an incidence angle of 70. The experimental data was fitted as described previously [33].

3. Results and discussion

3.1. Effect of the polyelectrolyte system and Pt precursor

We prepared Pt NPs from $\text{Pt}(\text{NH}_3)_4^{2+}$ or PtCl_6^{2-} in two model polyelectrolyte multilayer systems: PAH/PAA and PDDA/Nafion films. The chemical structures of the polyelectrolytes and the platinum complexes are depicted in Fig. 1. The first system (PAH/PAA) was chosen because it has been widely studied both from the fundamental point of view and as a NP nanoreactor [1,2,4]. The PDDA/Nafion is interesting because the known proton conductivity and chemical stability of Nafion. Moreover, direct methanol fuel cells use Nafion as a proton-conducting polymer, which is in intimate contact with the Pt catalyst during fuel cell operation, therefore it is interesting to test the compatibility of the nanoreactor scheme with this polyelectrolyte. Finally, both PDDA and Nafion are strong polyelectrolytes, while PAH and PAA are both weak polyelectrolytes and therefore their multilayer films can present unpaired amino and/or carboxylic groups [34]. The NH_2 and COO^- groups in PAH and PAA, respectively, are better bases and, thus, stronger ligands [35], than the NR_4^+ and SO_3^- in PDDA and Nafion.

The LbL films were constructed starting from the positive polyelectrolyte because graphite surfaces have acidic isoelectric points due to the presence of surface carboxylate groups [36]. The last adsorbed layer was chosen to have a charge of opposite sign to that of the Pt precursor in order to favor loading (Fig. 1d). We will follow in this work the nomenclature introduced by Rubner: [1] i.e. a film bearing \times PDDA/Nafion bilayers and exposed to n exchange/reduction cycles with $\text{Pt}(\text{NH}_3)_4^{2+}$ is denoted $(\text{PDDA/Nafion})_x + n \text{Pt}(\text{NH}_3)_4^{2+}$. Considering that transmission electron microscopy is difficult to perform over ultrathin organic films deposited on bulk carbon electrodes, we decided to use scanning electron microscopy (SEM) to determine the rough size of the PtNPs. Fig. 2 shows top-view FE-SEM images of Pt-loaded films. Images show the presence of well-distributed NPs of relatively low size polydispersity for all the systems under study. PtNPs

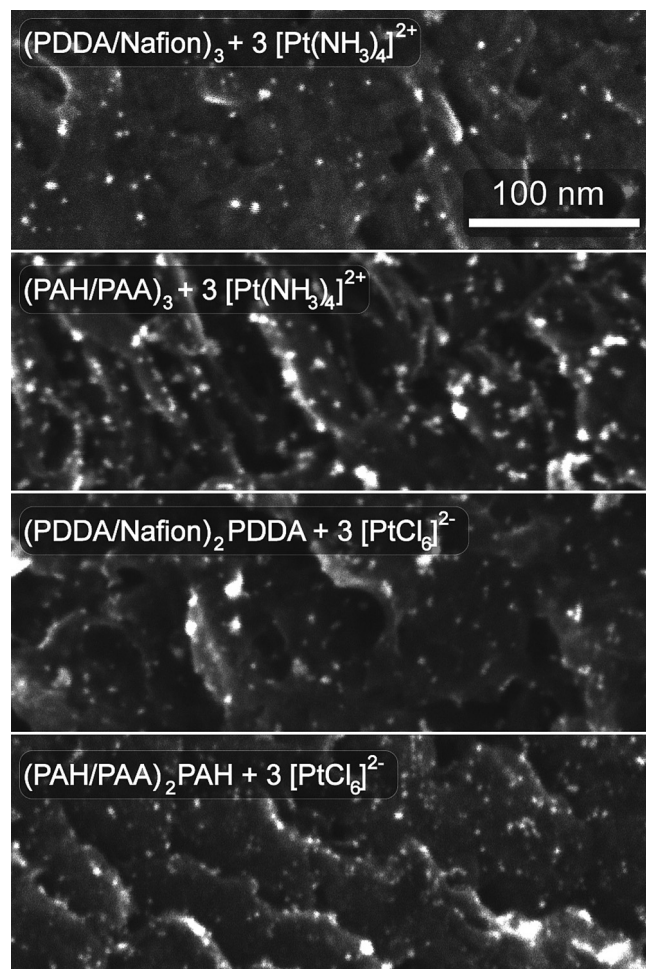


Fig. 2. SEM images for Pt NP-modified graphite electrodes based on different LbL films. The scale bar is the same for all images.

do not form aggregates and cover the surface of the electrode evenly. The surface density of particles is greater for the case of using PAH/PAA multilayers, and the sizes are about two times larger when using $\text{Pt}(\text{NH}_3)_4^{2+}$ in comparison with PtCl_6^{2-} .

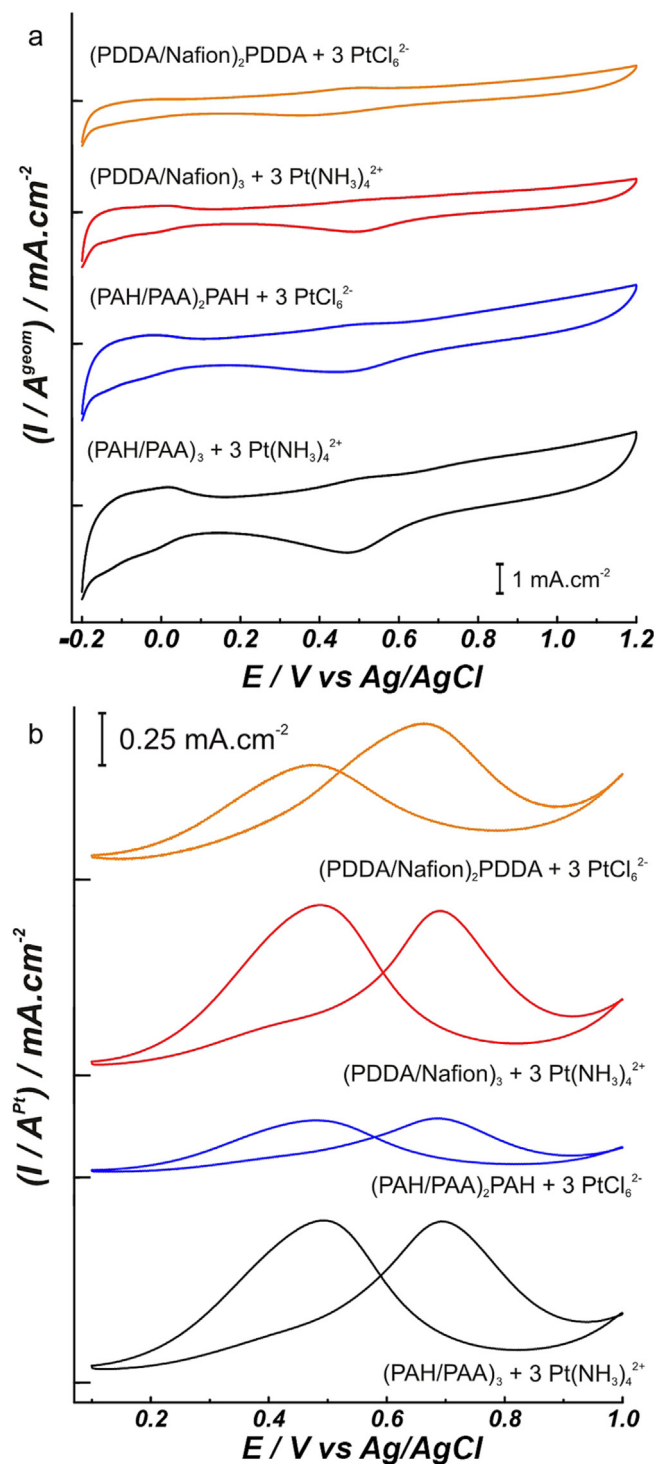


Fig. 3. a. Cyclic voltammograms measured in Ar-purged H_2SO_4 0.5 M for Pt-NP modified graphite electrodes based on different LbL films. The curves are normalized to the electrode geometric area. Scan rate: 0.1 V/s. b. MOR current-potential waves for Pt-NP modified graphite electrodes based on different LbL films. The curves correspond to the difference between the cyclic voltammograms in Ar-purged H_2SO_4 0.5 M + 1 M MeOH and the blank CV measured in Ar-purged H_2SO_4 0.5 M and are normalized by the Pt ECSA (A^{Pt}) determined from H_{upd} . Scan rate: 0.2 V/s.

Fig. 3a shows that the electrochemical behaviour of all systems under investigation is consistent with the presence of Pt. These voltammograms differ from that of a bare bulk polycrystalline Pt in the position of the platinum oxide reduction peak ($E_{\text{PtOx/Pt}}$) that is slightly shifted to cathodic potentials (i.e., the Pt oxide becomes more stable), see Fig. 4 and Table 1. This effect has been attributed in the literature to the decreasing in NP size [32,37], but we also observed a shift in the same direction upon polyelectrolyte adsorption on a bare Pt surface (see Fig. 4a and Table 1).

For each modified surface, we calculated the electrochemically active Pt surface area (ECSA, A^{Pt}) by hydrogen underpotential deposition (H_{upd}) assuming a specific charge of $210 \mu\text{C}\cdot\text{cm}^{-2}$ (Table 1) [38,39]. According to Xu and Shao-Horn, H_{upd} provides only an approximation of the ECSA [40], however, the aim of this work is to determine the effect of the multilayer identity on the electrochemical performance rather than comparing absolute values with related systems in literature. Then, H_{upd} gives a good estimation of the ECSA that allow us to compare between different polyelectrolyte systems. The fact that Pt NPs in PAH/PAA films have higher ECSAs than PDDA/Nafion ones (Table 1) is attributed to the fact that the film thickness of PAH/PAA (~8–10 nm/bilayer for the pH combination used in this work, see Fig. S1) is higher than that of PDDA/Nafion (3.2 nm/bilayer, see Fig. S2). This conclusion is supported by previous studies that report a negative correlation between the permanent charge density of the polyelectrolytes and their film thickness [41]. Therefore, for a fixed number of bilayers, the total Pt content of PAH/PAA films is higher than that of PDDA/PAA due to the different film thicknesses. An additional factor favoring NP loading in PAH/PAA films could be the presence of unpaired amine or carboxylic groups which, in principle, can bind the Pt precursor via ligand exchange. To decouple these two factors, we normalized the ECSA of each system by the film volume (Table 1). We observe that the volume-normalized ECSA is insensitive to the choice of the polyelectrolyte pair, which suggests that the composition of the film does not strongly affect the loading into the film of the precursor and its conversion to Pt NPs. Interestingly, when $\text{Pt}(\text{NH}_3)_4^{2+}$ was used in the loading procedure, the volume-normalized ECSA was 40 to 50% higher than in experiments using PtCl_6^{2-} .

The ratios of Pt ECSA to the geometric area of the electrode in Table 1 are higher than one, which seems to contrast with the sparse distribution of Pt NP in the SEM images of Fig. 2. This difference can be originated in i) the high roughness of the graphite substrate ii) the presence of Pt NP below the resolution limit and iii) the inability of SEM of imaging Pt NP far beneath film surface [9]. The feasibility of the latter explanation was demonstrated by the fact that increasing the number of Nafion/PDDA bilayers did not increase the density of Pt NP observed by SEM (for a constant number of exchange/reduction cycles). This result suggests that NPs inside the film are not detected by SEM, which is in agreement with previous SEM and XPS experiments for Pd NPs electrodeposited in LbL films from confined precursors [9], although in that case, NPs grew in the electrode/film interface and thus were only detectable by SEM for very thin polyelectrolyte films or after film delamination.

The current-potential waves in Fig. 3b show that all films under study are electrocatalytically active towards MOR in H_2SO_4 media. In order to allow comparison between the different systems, the currents in Fig. 3b are normalized by the ECSA. According to Manoharan and Goodenough, while the forward scan peak ($E \approx 0.68 \text{ V}_{\text{Ag/AgCl}}$ vs Ag/AgCl) is considered to be the main peak of the MOR, the backwards scan peak ($E \approx 0.48 \text{ V}_{\text{Ag/AgCl}}$ vs Ag/AgCl) corresponds to the oxidation of residual intermediates that were generated after methanol oxidation [42]. Also, Manoharan and Goodenough proposed that the ratio between the forward and the backward peak currents is somehow related with the level of CO-poisoning. In most recent reports, however, it was demonstrated that while indeed the forward scan peak current correspond to the oxidation of adsorbed methanol, the backwards

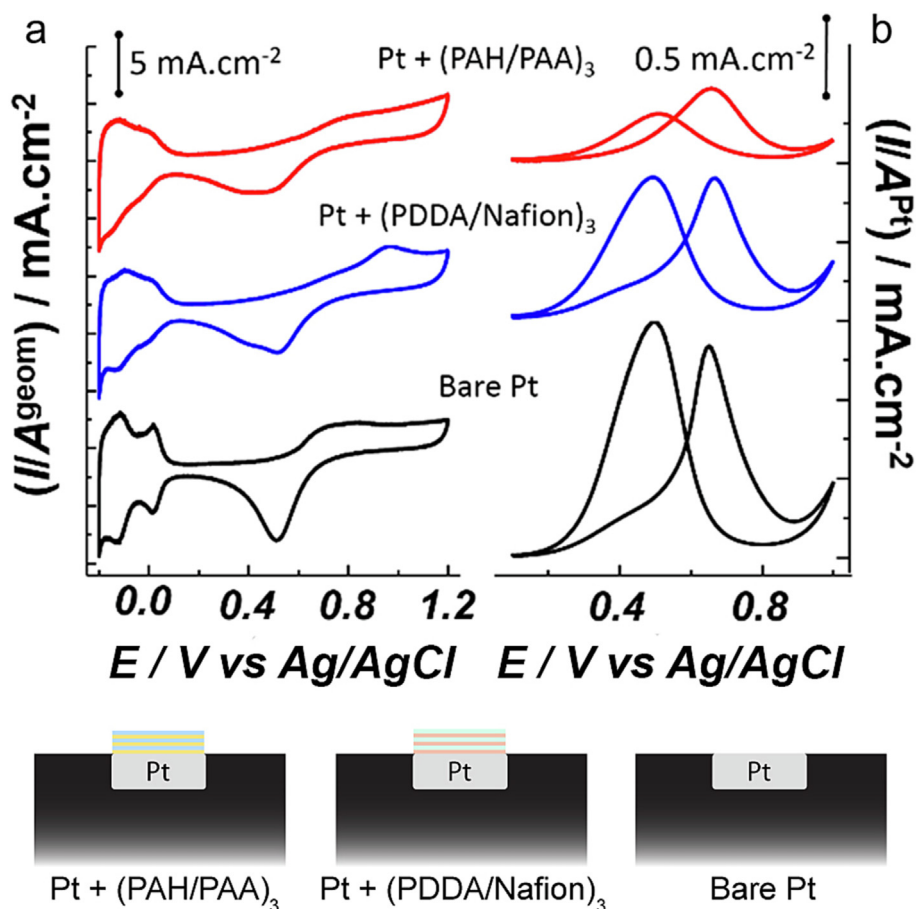


Fig. 4. a. cyclic voltammograms of a bare Pt bulk electrode and Pt bulk electrodes modified by PDDA/Nafion and PAH/PAA lbl film in Ar-purged H_2SO_4 0.5 M. The curves are normalized to the electrode geometric area. Scan rate: 0.1 V/s. b. MOR current-potential waves for the electrodes in a. The curves correspond to the difference between the cyclic voltammograms in Ar-purged H_2SO_4 0.5 M + 1 M MeOH and the blank CV measured in Ar-purged H_2SO_4 0.5 M and are normalized to the Pt ECSA (A^{Pt}) determined from H_{upd} . Scan rate: 0.2 V/s.

Table 1

Electrochemical data for different Pt NP-modified graphite surfaces obtained from the cyclic voltammetry analysis in Ar-saturated H_2SO_4 0.5 M with and without 1 M MeOH (MOR and Pt cyclic voltammetry, respectively). Results for a clean and a (PDDA/Nafion)₃-modified Pt bulk electrodes are also shown for comparison. *See CV in Fig. S3.

System	Pt cyclic voltammetry			Methanol electro-oxidation
	$E_{\text{PtOx/Pt}}(V_{\text{Ag/AgCl}})$	$\frac{A^{\text{Pt}}}{A^{\text{geom}}}$	$\frac{A^{\text{Pt}}}{V_{\text{Ox}}}(\text{nm}^{-1})$	$\frac{I}{A^{\text{Pt}}}$ at 0.68 $V_{\text{Ag/AgCl}}$ ($\text{mA}\cdot\text{cm}^{-2}$)
(PAH/PAA) ₃ + 3Pt(NH ₃) ₄ ²⁺	0.474	7.3	0.27	0.77
(PAH/PAA) ₂ PAH + 3 PtCl ₆ ²⁻	0.461	4.5	0.20	0.28
(PDDA/Nafion) ₃ + 3Pt(NH ₃) ₄ ²⁺	0.493	2.7	0.33	0.79
(PDDA/Nafion) ₂ PDDA + 3 PtCl ₆ ²⁻	0.384	1.1	0.22	0.70
Pt bulk	0.510	1.18		1.34
Pt bulk + (PDDA/Nafion) ₃	0.512, 0.416 (shoulder)*	0.79		0.82
Pt bulk + (PAH/PAA) ₃	0.434	0.93		0.47

scan peak current is not related to the residual intermediate CO but to the surface coverage of free Pt that is available for methanol reaction [43,44]. For this reason, we will measure the potentiality of the films as electrocatalysts by registering the MOR forward scan peak currents at 0.68 $V_{\text{Ag/AgCl}}$. Fig. 3b clearly shows that the specific activities for the electrodes prepared with Pt(NH₃)₄²⁺ are higher than those of electrodes prepared from PtCl₆²⁻, regardless of the multilayer architecture. This result has a probable cause in the inhibitory effect of chloride anions on MOR that is well known in the literature [45]. In line with this hypothesis, Cl was detected by XPS on the catalysts prepared from PtCl₆²⁻, although it is unknown whether this signal is originated from Cl⁻ adsorbed on the Pt NPs or from Pt complexes that failed to react during the chemical reduction step. The sample (PDDA/Nafion)₃ + 3-

Pt(NH₃)₄²⁺ had the highest specific activity for the MOR (see Table 1). The specific activity of this sample was smaller than that of a bulk Pt electrode, but similar to that of a bulk Pt electrode modified by a PDDA/Nafion multilayer film (see Table 1). This result indicates that the polymer/Pt interaction is detrimental to the activity of the catalysts prepared within the nanoreactors. Note, however, that due to the high surface-to-volume ratio of the NPs, the catalytic current normalized by the geometric area is still higher for the (PDDA/Nafion)₃ + 3Pt(NH₃)₄²⁺ film (2.4 $\text{mA}\cdot\text{cm}^{-2}$) than for the bulk Pt electrode (1.7 $\text{mA}\cdot\text{cm}^{-2}$). Moreover, in real fuel cell applications, Nafion is mixed with Pt on carbon catalyst in order to provide proton conductivity and therefore even uncoated Pt NPs are exposed to the effect of this polymer.

3.2. Effect of the number of exchange/reduction cycles

We chose the (PDDA/Nafion)₃ + *n* Pt(NH₃)₄²⁺ system for a detailed study of the effect of the number of exchange/reduction steps because it showed the highest specific activity for MOR. Fig. 5 shows SEM images for an increasing number of exchange/reduction cycles. The density of particles for *n* = 3 (i.e., three exchange/reduction cycles) is higher than that for *n* = 1, but the average particle size does not increase significantly (see Fig. S4). This suggests that during the first 3 exchange/reduction cycles, the nucleation of Pt NPs dominates over growing. For *n* = 5, both the number and size of NPs were larger than for *n* = 3 (see histograms in Fig. 5 and Fig. S4). This result contrasts with a previous report of Ag-loaded PAH/PAA films in which increasing the number of adsorption/reduction steps produced an increase in the size of NPs but not in their number [2]. In that case, it was proposed that the Ag NPs formed in the first cycle acted as seeds during the following reduction reactions. Our results can be put in line with this report if a large number of Pt seeds are formed during the first three cycles, followed by growing in the next cycles. Another possible explanation is that our (PDDA/Nafion)₃ + *n* Pt(NH₃)₄²⁺ films present a much lower NP content than the (PAA/PAH)_{*x*} + *n* Ag films of Ref 2

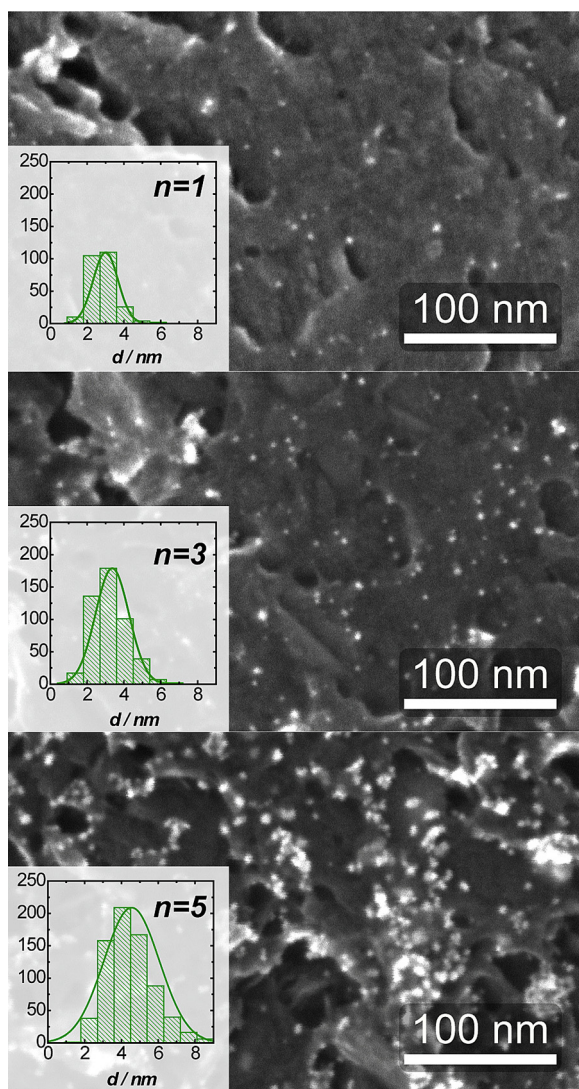


Fig. 5. SEM images acquired for (PDDA/Nafion)₃ + *n* Pt(NH₃)₄²⁺ films. The size histograms result from the analysis of three images taken from different regions of the sample, for each *n*.

and, therefore, the nucleation of confined Pt(NH₃)₄²⁺ ions is favored over their lateral diffusion through the film and deposition on preexistent Pt NPs in the early stages of Pt NP formation.

The surface composition of (PDDA/Nafion)₃ + *n* Pt(NH₃)₄²⁺ films was analyzed with XPS. In all cases, we analyzed the S2*p* and F1*s* signals at 688.6 and 169.1 eV (from Nafion) and the N1*s* peak at 400.4 eV (from PDDA). For *n* > 0 we also analyzed the Pt4*f* region that was fitted using two components located at 71.1 and 72.1 eV (position of Pt4*f*_{5/2}), assigned to metallic Pt(0) and Pt(II) respectively [46]. Table 2 shows that the total amount of Pt (given by the (Pt(0) + Pt(II))/S ratio) increases with *n*, as expected, and that the fraction of Pt(0) is in the range 0.64–0.79 indicating that either some Pt ions were not reduced by BH₄⁻ or that Pt NPs suffer oxidation in air. A similar reduction efficiency has been observed for Pd NPs prepared in LbL films by NaBH₄ reduction [20]. Interestingly, the fraction of Pt(0) decrease with increasing *n*. Within each exchange/reduction cycle, the sample is immersed in a Pt precursor solution for 24 h followed by NaBH₄ reduction. As *n* becomes bigger, it seems like the reduction step becomes more and more ineffective. This effect may be due to an accumulation of Pt(II) ions that are inaccessible to BH₄⁻ ions. From the Pt/S, N/S and F/S relationships it is possible to roughly estimate the volume fraction of Pt in the film (assuming that XPS is probing all the atoms in the film with the same sensitivity and a density for the polymers of 1.5 g/cm³). The as-calculate volume fractions ranged from 0.4 % (for *n* = 1) to 3 % (for *n* = 5) which is in qualitative agreement with the low coverage observed in the SEM images. With this data we can roughly estimate the Pt loading mass within the LbL which will be around 0.5 pg/cm² for *n* = 5.

Fig. 6a shows the cyclic voltammetry of the films under study in methanol-free H₂SO₄. Upon increasing the number of exchange/reduction cycles, the CV develops features in the hydrogen and Pt oxide regions that are typically observed for Pt bulk electrodes. Fig. 6b shows the normalized Pt ECSA for increasing exchange/reduction cycles. In concordance with the trend observed for the number of Pt NPs observed by SEM, the Pt ECSA increases monotonically with the number of exchange/reduction cycles. Fig. 6 also shows that the position of *E*_{PtOx/Pt} shifts toward positive potentials as the number of exchange/reduction cycles increases and reaches a constant value of ~ 0.5 V_{Ag/AgCl} for *n* ≥ 3 (Fig. 6c). This value is close to the position of the *E*_{PtOx/Pt} peak in the cyclic voltammetry of clean Pt bulk electrode (dashed line in Fig. 6c). The shift of the *E*_{PtOx/Pt} peak with *n* may result from changes in particle size [37]; however this effect cannot fully explain the observation because the particle size increases with *n* for *n* > 3 (inset in Fig. 5), while *E*_{PtOx/Pt} reaches a constant value in those conditions (Fig. 6c).

An alternative explanation for the effect of *n* on the position of *E*_{PtOx/Pt} could be the presence of polymer-Pt interactions. The reduction of Pt oxide for (PDDA/Nafion)₃-coated Pt bulk electrode (see Fig. S3) results in a peak at ~ 0.5 V_{Ag/AgCl} (i.e., the same potential as for a bare Pt electrode) with a shoulder at ~ 0.42 V_{Ag/AgCl}, which can be attributed to surface sites interacting with the polymers [47]. We believe that the polymer-NP interaction may play a similar effect in the case of the Pt NPs, shifting the position of *E*_{PtOx/Pt} towards negative potentials. In

Table 2

XPS atomic ratios for a (PDDA/Nafion)₃ + *n* Pt(NH₃)₄²⁺ modified graphite electrode.

Atomic ratio	<i>n</i> = 0	<i>n</i> = 1	<i>n</i> = 3	<i>n</i> = 5
F/S	21.70	24.41	29.01	26.14
N(PDDA)/S	0.39	2.27	0.98	0.73
N(total)/S	1.14	2.75	2.35	1.58
Pt/S	0	0.32	0.56	1.90
Pt (0)/Pt(total)	–	0.79	0.76	0.64
F/C (Nafion)	2.72	2.55	2.06	2.15

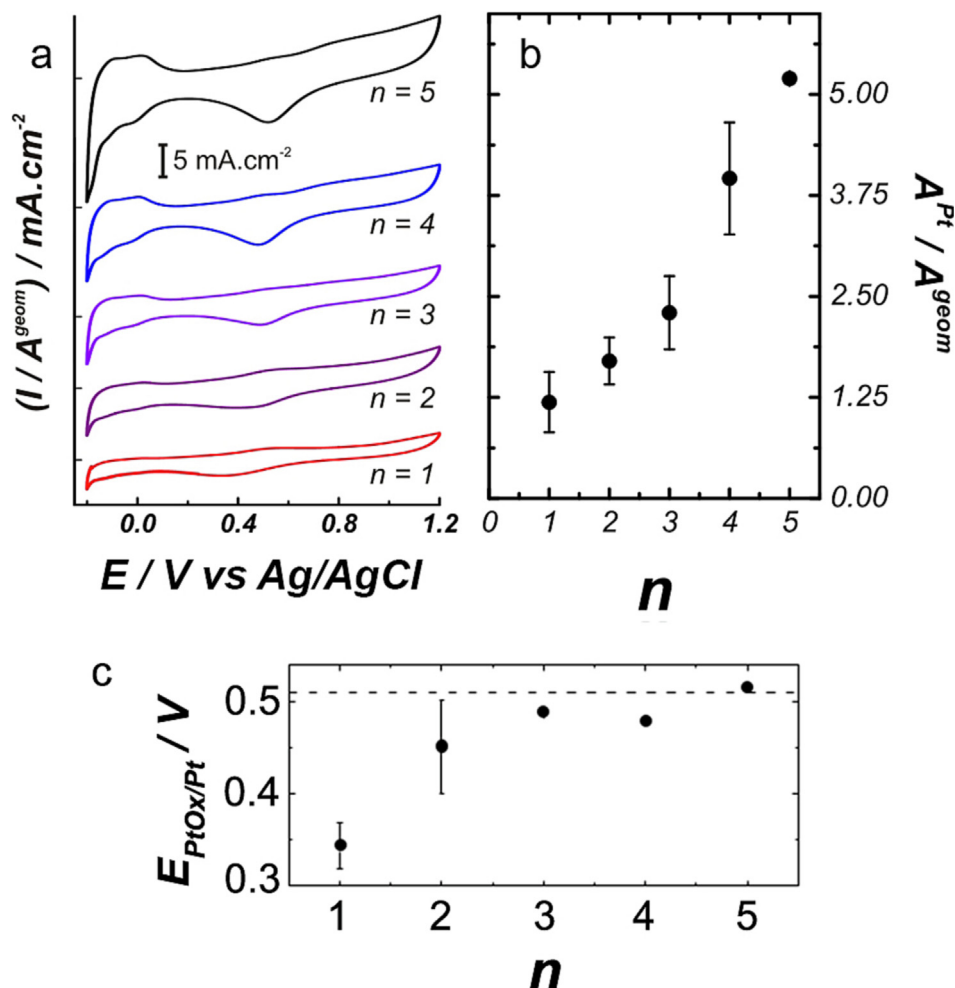


Fig. 6. a. Cyclic voltammograms normalized to the electrode geometric area for $(\text{pdda/nafion})_3 + n \text{Pt}(\text{NH}_3)_4^{2+}$ (with n the number of exchange/reduction cycles) in Ar-purged H_2SO_4 0.5 M. b. Pt ECSA (A^{Pt}) determined by H_{upd} normalized to the electrode geometric area as a function of the exchange/reduction cycles. c. Position of the $E_{\text{PtOx/Pt}}$ peak as a function of the number of exchange/reduction cycles. The dashed line shows the potential for a bare bulk Pt electrode. In panels b and c, each point corresponds to measurements on 3 independent electrodes; the error bars show one standard deviation.

that scenario, the fact that $E_{\text{PtOx/Pt}}$ gets close to the value of a bare Pt bulk with increasing n indicates that the fraction of Pt sites interacting with the polymer in the NPs decreases with increasing number of exchange/reduction cycles.

Fig. 7a shows that the MOR current increases with the number of adsorption/reduction cycles. The anodic peak current at $0.68 \text{ V}_{\text{Ag/AgCl}}$ linearly increases with the number of exchange/reduction cycles (Fig. 7b). This linear increase is in concordance with the observed evolution of particle size and density (Fig. 5).

However, after normalization by the Pt ECSA (Fig. 8), an interesting behavior is observed: the catalytic activity increases with the number of exchange/reduction cycles up to $n = 2$ and then reaches a constant value that is close to that measured for a $(\text{PDDA}/\text{Nafion})_3$ -coated Pt bulk electrode (see Table 1). This behavior is very similar to that observed in Fig. 6c, which was ascribed to the effect of polymer-surface interactions. Interestingly, assembling a $(\text{PDDA}/\text{Nafion})_3$ film on top of a Pt electrode reduces its specific activity toward MOR to around a half of that of the bare Pt surface (Fig. 4b and Table 1).

Considered together, these results suggest that the specific activity in the multilayer-embedded Pt NPs is mainly modulated by the polymer-surface interactions. For $n \leq 2$, the specific activity and $E_{\text{PtOx/Pt}}$ (Fig. 6c) increase with n because there is a decrease in the strength and/or extent of the polymer-NPs interactions. For $n > 2$, both the

specific activity (Fig. 8b) and $E_{\text{PtOx/Pt}}$ (Fig. 6c) become independent of the number of adsorption/reduction cycles. Note, that in this regime, the loading of Pt NPs still increases with n and, therefore, the activity per geometric area of electrode increases linearly with the number of exchange/reduction cycles (Fig. 7). Therefore, in order to obtain the maximum catalytic activity, the surface must be exposed to a at least 2 exchange/reduction cycles.

In summary, we observed that the nature of the polymers in the multilayer (*i.e.*, PDDA/Nafion vs PAH/PAA films) has little effect on the electroactive area of Pt, once the different thicknesses of the two different polyelectrolyte systems were considered. Therefore, the free carboxylates and amino groups in PAH/PAA film do not appear to strongly contribute to complex uptake, which suggests that the main driving force for the incorporation of Pt complexes into the film is the electrostatic interaction between the charged polymer residues and Pt precursors. On the other hand, for the same polyelectrolyte-pair, Pt NPs prepared from $\text{Pt}(\text{NH}_3)_4^{2+}$ showed higher electroactive area and higher specific activity for MOR than NPs prepared with PtCl_6^{2-} . These results may be explained by the strong adsorption of chloride ions on Pt surfaces [45]. Notably, all previous work using LbL nanoreactors to grow Pt NPs used the less effective precursors, PtCl_6^{2-} [24,25]. For the system $(\text{PDDA}/\text{Nafion})_3 + n \text{Pt}(\text{NH}_3)_4^{2+}$ we observed that the MOR current normalized by the Pt ECSA increased linearly with n for $n \leq 2$. Under those conditions, the potential of the Pt reduc-

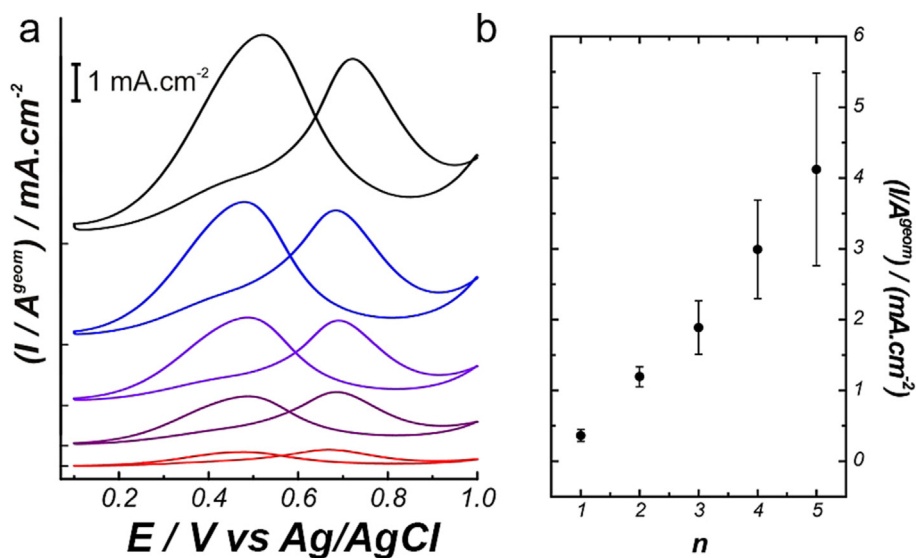


Fig. 7. a. MOR current–potential waves for $(PDDA/Nafion)_3 + n Pt(NH_3)_4^{2+}$ electrodes (blank subtracted) normalized to the geometrical area of the electrode in Ar-purged H_2SO_4 0.5 M + 1 M MeOH. b. MOR current at $E = 0.68 V_{Ag/AgCl}$ normalized to the electrode geometrical area as a function of the exchange/reduction cycles. Each point corresponds to measurements on 3 independent electrodes; the error bars show one standard deviation.

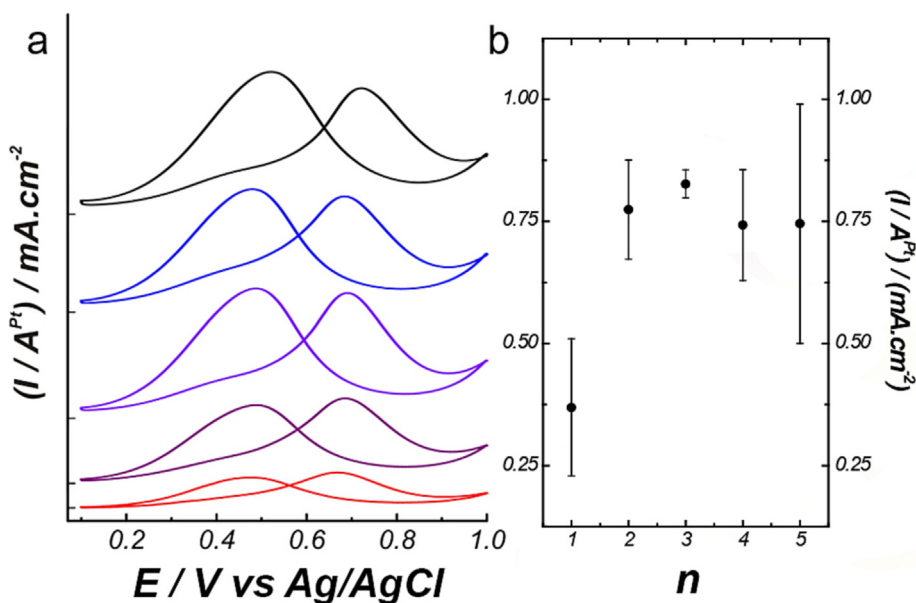


Fig. 8. a. MOR current–potential waves for $(PDDA/Nafion)_3 + n Pt(NH_3)_4^{2+}$ electrodes (blank subtracted) normalized to the geometrical electrode area in Ar-purged H_2SO_4 0.5 M + 1 M MeOH. b. MOR current at $E = 0.68 V_{Ag/AgCl}$ as a function of n normalized to the Pt ECSA (A^{Pt}) determined by H_{upd} . The current value for each point corresponds to measurements on 3 independent electrodes.

tion peak in the voltammetry shifts towards anodic potentials. For $n > 2$, both parameters reached a stable value and the reduction potential of Pt oxide approaches that of a bare Pt bulk electrode. Moreover, assembling a PDDA/Nafion film on top of the bare Pt electrode results both in a decrease of the specific activity for MOR and a shift of the potential of Pt oxide reduction. Taken together, these results suggest that there is a strong polymer-surface interaction which decreases with increasing n and stabilizes for $n > 2$. It is difficult to establish a definitive mechanism by which successive exchange/reduction cycles decrease the polymer/surface interaction in the system. We propose that small particles may exhibit a larger density of surface defects than large ones and, therefore, be more prone to interact with

the polymers. Alternatively, the mechanical stresses that should arise during the growth of NPs might detach the polymer chains from the surface.

4. Conclusions

In the present work we systematically investigated the effect of the type of multilayer film, Pt precursor complex and number of exchange/reduction cycles in the construction and electrocatalytic performance towards MOR of Pt NP-containing polyelectrolyte films supported on graphite. Employing the LbL methodology followed by

successive exchange/reduction cycles we obtained Pt NPs with average sizes between 3 and 4 nm and excellent catalytic activity.

The Pt precursors and polyelectrolyte-pairs used in this work can be extended to different carbonaceous materials such as carbon Vulcan, graphene and carbon nanotubes for the construction of new direct methanol fuel cells. We demonstrated that polymer-NP interactions have an inhibitory effect on the electrocatalytic activity. This deleterious effect can be decreased by a proper choice of the polyelectrolyte pair and by increasing the number of exchange/reduction cycles. These results put in evidence that the modification of the catalytic activity of embedded NPs by the polyelectrolyte matrix is a ubiquitous, although seldom discussed, characteristic of the nanoreactor strategy.

CRedit authorship contribution statement

Santiago E. Herrera: Conceptualization, Methodology, Investigation, Writing – original draft, Writing – review & editing, Visualization, Supervision, Funding acquisition. **Mario Tagliazucchi:** Conceptualization, Methodology, Investigation, Writing – original draft, Visualization, Supervision, Funding acquisition. **Federico J. Williams:** Methodology, Investigation, Writing – original draft, Visualization. **Ernesto J. Calvo:** Conceptualization, Methodology, Resources, Writing – original draft, Supervision, Project administration.

Declaration of Competing Interest

The authors declare that they have no known competing financial interests or personal relationships that could have appeared to influence the work reported in this paper.

Acknowledgments

S.E.H., F.J.W., E.J.C. and M.T. are Fellows of CONICET. We acknowledge financial support from CONICET (grant number PIP 53311220200102008CO, PIP 11220200102008CO, and PIBBA 28720210100613CO) and Agencia Nacional de Promoción Científica y Tecnológica (grant number PICT 1758-2020, PICT 0035-2020, PICT 4649-2018, and PICT 1520-2019).

Appendix A. Supplementary data

Supplementary data to this article can be found online at <https://doi.org/10.1016/j.jelechem.2023.117430>.

References

- [1] S. Joly, R. Kane, L. Radzilowski, T. Wang, A. Wu, R.E. Cohen, E.L. Thomas, M.F. Rubner, Multilayer nanoreactors for metallic and semiconducting particles, *Langmuir* 16 (2000) 1354–1359, <https://doi.org/10.1021/la991089t>.
- [2] T.C. Wang, M.F. Rubner, R.E. Cohen, Polyelectrolyte multilayer nanoreactors for preparing silver nanoparticle composites: controlling metal concentration and nanoparticle size, *Langmuir* 18 (2002) 3370–3375, <https://doi.org/10.1021/la015725a>.
- [3] J. Dai, M.L. Bruening, Catalytic nanoparticles formed by reduction of metal ions in multilayered polyelectrolyte films, *Nano Lett.* 2 (2002) 497–501, <https://doi.org/10.1021/nl025547l>.
- [4] K.-K. Chia, R.E. Cohen, M.F. Rubner, Amine-rich polyelectrolyte multilayer nanoreactors for in situ gold nanoparticle synthesis, *Chem. Mater.* 20 (2008) 6756–6763, <https://doi.org/10.1021/cm802166s>.
- [5] D. Lee, R.E. Cohen, M.F. Rubner, Antibacterial properties of Ag nanoparticle loaded multilayers and formation of magnetically directed antibacterial microparticles, *Langmuir* 21 (2005) 9651–9659, <https://doi.org/10.1021/la0513306>.
- [6] Z. Li, D. Lee, X. Sheng, R.E. Cohen, M.F. Rubner, Two-level antibacterial coating with both release-killing and contact-killing capabilities, *Langmuir* 22 (2006) 9820–9823, <https://doi.org/10.1021/la0622166>.
- [7] S. Kidambi, J. Dai, J. Li, M.L. Bruening, Selective hydrogenation by Pd nanoparticles embedded in polyelectrolyte multilayers, *J. Am. Chem. Soc.* 126 (2004) 2658–2659, <https://doi.org/10.1021/ja038804c>.
- [8] S. Bhattacharjee, D.M. Dotzauer, M.L. Bruening, Selectivity as a function of nanoparticle size in the catalytic hydrogenation of unsaturated alcohols, *J. Am. Chem. Soc.* 131 (2009) 3601–3610, <https://doi.org/10.1021/ja807415k>.
- [9] M. Vago, M. Tagliazucchi, F.J. Williams, E.J. Calvo, Electrodeposition of a palladium nanocatalyst by ion confinement in polyelectrolyte multilayers, *Chem. Commun.* (2008) 5746, <https://doi.org/10.1039/b812181h>.
- [10] J. Choi, M.F. Rubner, Influence of the degree of ionization on weak polyelectrolyte multilayer assembly, *Macromolecules* 38 (2005) 116–124, <https://doi.org/10.1021/ma048596o>.
- [11] S. Liang, W. Yan, X. Wu, Y. Zhang, Y. Zhu, H. Wang, Y. Wu, Gel polymer electrolytes for lithium ion batteries: fabrication, characterization and performance, *Solid State Ion.* 318 (2018) 2–18, <https://doi.org/10.1016/j.ssi.2017.12.023>.
- [12] M. Tagliazucchi, F.J. Williams, E.J. Calvo, Metal-ion responsive redox polyelectrolyte multilayers, *Chem. Commun.* 46 (2010) 9004, <https://doi.org/10.1039/c0cc02738c>.
- [13] T. Zhu, Y. Sha, J. Yan, P. Pageni, M.A. Rahman, Y. Yan, C. Tang, Metallo-polyelectrolytes as a class of ionic macromolecules for functional materials, *Nat. Commun.* 9 (2018) 4329, <https://doi.org/10.1038/s41467-018-06475-9>.
- [14] D.K. Beaman, E.J. Robertson, G.L. Richmond, Metal ions: driving the orderly assembly of polyelectrolytes at a hydrophobic surface, *Langmuir* 28 (2012) 14245–14253, <https://doi.org/10.1021/la302917p>.
- [15] A. Mentbayeva, A. Ospanova, Z. Tashmuhambetova, V. Sokolova, S. Sukhishvili, Polymer-metal complexes in polyelectrolyte multilayer films as catalysts for oxidation of toluene, *Langmuir* 28 (2012) 11948–11955, <https://doi.org/10.1021/la302534z>.
- [16] W.S. Choi, H.Y. Koo, J.-H. Park, D.-Y. Kim, Synthesis of two types of nanoparticles in polyelectrolyte capsule nanoreactors and their dual functionality, *J. Am. Chem. Soc.* 127 (2005) 16136–16142, <https://doi.org/10.1021/ja053981u>.
- [17] Y. Shen, J. Liu, A. Wu, J. Jiang, L. Bi, B. Liu, Z. Li, S. Dong, Preparation of multilayer films containing Pt nanoparticles on a glassy carbon electrode and application as an electrocatalyst for dioxygen reduction, *Langmuir* 19 (2003) 5397–5401, <https://doi.org/10.1021/la020845j>.
- [18] H. Li, L.-P. Jia, R.-N. Ma, W.-L. Jia, H.-S. Wang, Electrodeposition of PtNPs on the LBL assembled multilayer films of (PDDA-GS/PEDOT:PSS) n and their electrocatalytic activity toward methanol oxidation, *RSC Adv.* 7 (2017) 16371–16378, <https://doi.org/10.1039/C6RA28784K>.
- [19] K.R. Knowles, C.C. Hanson, A.L. Fogel, B. Warhol, D.A. Rider, Layer-by-layer assembled multilayers of polyethylenimine-stabilized platinum nanoparticles and PEDOT:PSS as anodes for the methanol oxidation reaction, *ACS Appl. Mater. Interfaces* 4 (2012) 3575–3583, <https://doi.org/10.1021/am300639z>.
- [20] S. Kidambi, M.L. Bruening, Multilayered polyelectrolyte films containing palladium nanoparticles: synthesis, characterization, and application in selective hydrogenation, *Chem. Mater.* 17 (2005) 301–307, <https://doi.org/10.1021/cm048421t>.
- [21] C. Chu, Z. Su, Gold-decorated platinum nanoparticles in polyelectrolyte multilayers with enhanced catalytic activity for methanol oxidation, *Appl. Catal. A Gen.* 517 (2016) 67–72, <https://doi.org/10.1016/j.apcata.2016.03.002>.
- [22] C. Chu, Z. Su, Facile synthesis of AuPt alloy nanoparticles in polyelectrolyte multilayers with enhanced catalytic activity for reduction of 4-nitrophenol, *Langmuir* 30 (2014) 15345–15350, <https://doi.org/10.1021/la5042019>.
- [23] X. Zhang, Z. Su, Polyelectrolyte-multilayer-supported Au@Ag core-shell nanoparticles with high catalytic activity, *Adv. Mater.* 24 (2012) 4574–4577, <https://doi.org/10.1002/adma.201201712>.
- [24] X. Zhang, X. Zan, Z. Su, Polyelectrolyte multilayer supported Pt nanoparticles as catalysts for methanol oxidation, *J. Mater. Chem.* 21 (2011) 17783, <https://doi.org/10.1039/c1jm12892b>.
- [25] Z. Wang, G. Zhang, Z. Zhong, Y. Lin, Z. Su, In-situ synthesis of platinum nanoclusters in polyelectrolyte multilayer films, *Thin Solid Films* 660 (2018) 59–64, <https://doi.org/10.1016/j.tsf.2018.05.051>.
- [26] D. Xiao, Q. Jiang, C. Xu, C. Yang, L. Yang, H. He, H. Huang, Interfacial engineering of worm-shaped palladium nanocrystals anchored on polyelectrolyte-modified MXene nanosheets for highly efficient methanol oxidation, *J. Colloid Interface Sci.* 616 (2022) 781–790, <https://doi.org/10.1016/j.jcis.2022.02.111>.
- [27] W. Meng, H. He, L. Yang, Q. Jiang, B. Yuliarto, Y. Yamauchi, X. Xu, H. Huang, 1D–2D hybridization: nanoarchitectonics for grain boundary-rich platinum nanowires coupled with MXene nanosheets as efficient methanol oxidation electrocatalysts, *Chem. Eng. J.* 450 (2022) 137932, <https://doi.org/10.1016/j.cej.2022.137932>.
- [28] C. Yang, Q. Jiang, H. Liu, L. Yang, H. He, H. Huang, W. Li, Pt-on-Pd bimetallic nanodendrites stereoassembled on MXene nanosheets for use as high-efficiency electrocatalysts toward the methanol oxidation reaction, *J. Mater. Chem. A Mater.* 9 (2021) 15432–15440, <https://doi.org/10.1039/D1TA01784E>.
- [29] J. Qin, H. Huang, J. Zhang, F. Zhu, L. Luo, C. Zhang, L. Yang, Q. Jiang, H. He, Stereoassembly of ultrasmall Rh-decorated zeolite imidazolate framework–MXene heterostructures for boosted methanol oxidation reaction, *J. Mater. Chem. A Mater.* 11 (2023) 2848–2856, <https://doi.org/10.1039/D2TA08709J>.
- [30] C. Coutanceau, S. Brimaud, C. Lamy, J.-M. Léger, L. Dubau, S. Rousseau, F. Vigier, Review of different methods for developing nanoelectrocatalysts for the oxidation of organic compounds, *Electrochim. Acta* 53 (2008) 6865–6880, <https://doi.org/10.1016/j.electacta.2007.12.043>.
- [31] T. Biegler, D.A.J. Rand, R. Woods, Limiting oxygen coverage on platinumized platinum; Relevance to determination of real platinum area by hydrogen adsorption, *J. Electroanal. Chem. Interfacial Electrochem.* 29 (1971) 269–277, [https://doi.org/10.1016/S0022-0728\(71\)80089-X](https://doi.org/10.1016/S0022-0728(71)80089-X).

- [32] M. Arenz, K.J.J. Mayrhofer, V. Stamenkovic, B.B. Blizanac, T. Tomoyuki, P.N. Ross, N.M. Markovic, The effect of the particle size on the kinetics of CO electrooxidation on high surface area Pt catalysts, *J. Am. Chem. Soc.* 127 (2005) 6819–6829, <https://doi.org/10.1021/ja043602h>.
- [33] E.S. Forzani, M. Otero, M.A. Pérez, M.L. Teijelo, E.J. Calvo, The structure of layer-by-layer self-assembled glucose oxidase and Os(Bpy) 2 ClPyCH 2 NH–Poly (allylamine) multilayers: ellipsometric and quartz crystal microbalance studies, *Langmuir* 18 (2002) 4020–4029, <https://doi.org/10.1021/la025507x>.
- [34] M. Tagliazucchi, F.J. Williams, E.J. Calvo, Effect of acid–base equilibria on the donnan potential of layer-by-layer redox polyelectrolyte multilayers, *J. Phys. Chem. B* 111 (2007) 8105–8113, <https://doi.org/10.1021/jp071867n>.
- [35] F. Basolo, R.C. Johnson, *Coordination chemistry, Sci. Rev.* (1986).
- [36] R. Koestner, Y. Roiter, I. Kozhinova, S. Minko, Effect of local charge distribution on graphite surface on nafion polymer adsorption as visualized at the molecular level, *J. Phys. Chem. C* 115 (2011) 16019–16026, <https://doi.org/10.1021/jp203392m>.
- [37] Y. Takasu, Y. Fujii, K. Yasuda, Y. Iwanaga, Y. Matsuda, Electrochemical properties of ultrafine platinum particles for hydrogen electrode reaction in an aqueous solution of sulfuric acid, *Electrochim. Acta* 34 (1989) 453–458, [https://doi.org/10.1016/0013-4686\(89\)87025-2](https://doi.org/10.1016/0013-4686(89)87025-2).
- [38] K.J.J. Mayrhofer, D. Strmcnik, B.B. Blizanac, V. Stamenkovic, M. Arenz, N.M. Markovic, Measurement of oxygen reduction activities via the rotating disc electrode method: from Pt model surfaces to carbon-supported high surface area catalysts, *Electrochim. Acta* 53 (2008) 3181–3188, <https://doi.org/10.1016/j.electacta.2007.11.057>.
- [39] T. Binninger, E. Fabbri, R. Kötz, T.J. Schmidt, Determination of the electrochemically active surface area of metal-oxide supported platinum catalyst, *J. Electrochem. Soc.* 161 (2014) H121–H128. doi: 10.1149/2.055403jes.
- [40] C. Wei, R.R. Rao, J. Peng, B. Huang, I.E.L. Stephens, M. Risch, Z.J. Xu, Y. Shao-Horn, Recommended practices and benchmark activity for hydrogen and oxygen electrocatalysis in water splitting and fuel cells, *Adv. Mater.* 31 (2019) 1806296, <https://doi.org/10.1002/adma.201806296>.
- [41] E. Kharlampieva, S.A. Sukhishvili, Ionization and pH stability of multilayers formed by self-assembly of weak polyelectrolytes, *Langmuir* 19 (2003) 1235–1243, <https://doi.org/10.1021/la026546b>.
- [42] R. Mancharan, J.B. Goodenough, Methanol oxidation in acid on ordered NiTi, *J. Mater. Chem.* 2 (1992) 875, <https://doi.org/10.1039/jm9920200875>.
- [43] A.M. Hofstead-Duffy, D.-J. Chen, S.-G. Sun, Y.J. Tong, Origin of the current peak of negative scan in the cyclic voltammetry of methanol electro-oxidation on Pt-based electrocatalysts: a revisit to the current ratio criterion, *J. Mater. Chem.* 22 (2012) 5205, <https://doi.org/10.1039/c2jm15426a>.
- [44] D.Y. Chung, K.-J. Lee, Y.-E. Sung, Methanol electro-oxidation on the Pt surface: revisiting the cyclic voltammetry interpretation, *J. Phys. Chem. C* 120 (2016) 9028–9035, <https://doi.org/10.1021/acs.jpcc.5b12303>.
- [45] M.W. Breiter, Voltammetric study of the inhibition of methanol oxidation on platinum by chloride ion in acid solution, *Electrochim. Acta* 9 (1964) 827–833, [https://doi.org/10.1016/0013-4686\(64\)80068-2](https://doi.org/10.1016/0013-4686(64)80068-2).
- [46] P.K. Sahoo, R. Aepuru, H.S. Panda, D. Bahadur, Ice-templated synthesis of multifunctional three dimensional graphene/noble metal nanocomposites and their mechanical, electrical, catalytic and electromagnetic shielding properties, *Sci. Rep.* 5 (2016) 17726, <https://doi.org/10.1038/srep17726>.
- [47] J.-Y. Ye, G.A. Attard, A. Brew, Z.-Y. Zhou, S.-G. Sun, D.J. Morgan, D.J. Willock, Explicit detection of the mechanism of platinum nanoparticle shape control by polyvinylpyrrolidone, *J. Phys. Chem. C* 120 (2016) 7532–7542, <https://doi.org/10.1021/acs.jpcc.5b10910>.